Laser and Particle Beams (2012), *30*, 575–582.

doi:10.1017/S0263034612000547

Laser wakefield bubble regime acceleration of electrons in a preformed non uniform plasma channel

K.K. MAGESH KUMAR AND V.K. TRIPATHI
Physics Department, Indian Institute of Technology Delhi, New Delhi, India
(RECEIVED 10 April 2012; ACCEPTED 6 July 2012)

Abstract

A model of bubble regime electron acceleration by an intense laser pulse in non uniform plasma channel is developed. The plasma electrons at the front of the pulse and slightly off the laser axis in the plasma channel, experience axial and radial ponderomotive and space charge forces, creating an electron evacuated non uniform ion bubble. The expelled electrons travel along the surface of the bubble and reach the stagnation point, forming an electron sphere of radius r_e. The electrons of this sphere are pulled into the ion bubble and are accelerated to high energies. The Lorentz boosted frame enabled us to calculate energy gain of a test electron inside the bubble.

Keywords: Plasma channel; Pondermotive force; Stagnation point; Wakefield

1. INTRODUCTION

Electron plasma wave is recognized as a suitable high gradient accelerating structure for electron acceleration (Tajima & Dawson, 1979). An intense laser pulse ($I \geq 10^{18}$ W/cm^2) of duration ω_p^{-1}, propagating through a plasma of plasma frequency ω_p, can excite a large amplitude plasma wave in its wake with phase velocity equal to the group velocity of the laser. Energetic electrons that are trapped in the proper phase of the plasma wave are accelerated to very high energies by the axial electric field of the wave (Faure *et al.*, 2004; Hogan *et al.*, 2005; Chen *et al.*, 2008; Glinec *et al.*, 2005; Sadighi-Bonabi *et al.*, 2009). A large number of experiments and particle-in-cell (PIC) simulations (Esarey *et al.*, 2009; Pukhov & Meyer-ter-vehn *et al.*, 2002; Lu *et al.*, 2006) have confirmed the efficacy of this scheme of laser wakefield acceleration (LWFA) (Amiranoff *et al.*, 1998; Maksimchuk *et al.*, 2008; Siders *et al.*, 1996).

At relativistically high laser intensity and small spot size, the character of plasma wave changes dramatically. The laser pulse expels all the electrons from the axial region, through axial and radial ponderomotive force, creating a co-moving ion bubble. Reitsma and Jaroszynski (2004) have studied the coupling of longitudinal and transverse motion and electron acceleration in a laser wakefield accelerator. Balakirev *et al.* (2004) have reported via numerical simulation charged particle acceleration by an intense wakefield relativistic electron bunch. Dahiya *et al.* (2010) used 3D VORPAL CODE to study the self injection of electrons by exciting slow moving plasma wave in a ripple density plasma. They showed that the accelerated trapped electrons gained an average energy of about 40 MeV. Krishnagopal *et al.* (2011) have studied the self-injection of electrons for different intensity regimes and obtained good beam quality with injection of on-axis electrons. Gorbunov *et al.* (2005), used petawatt ultrashort laser pulses to study the evolution of wakefield, laser pulse, and the acceleration of injected electron bunches. PIC simulation have allowed to analyze the complex behavior of the bubble scenario in a systematic way, which led to the refinement of scaling laws valid under relativistic (Lu *et al.*, 2007) ($a_0 \geq 1$) and ultra-relativistic (Geddes *et al.*, 2004) ($a_0 \gg 1$) conditions.

Many of the studies on laser driven electron acceleration employ preformed plasma channels. Verma and Sharma (2011*a*, 2011*b*) have studied plasma channel formation by a laser pre-pulse in a low Z gas and also examined the nonlinear Eigen modes of a laser in a self created magnetized plasma channel under the combined effects of ponderomotive and relativistic mass nonlinearities. Singh and Singh (2011*a*, 2011*b*) have investigated the effect of relativistic nonlinearity on the guiding of a laser beam in an axially non-uniform plasma channel. Martins *et al.* (2010) have observed electron beams with narrow energy spread in preformed plasma channels using 1.4 PW laser. Sprangle *et al.* (2001) used tapered plasma channel for laser wakefield generation and electron

Address correspondence and reprint requests to: K.K. Magesh Kumar, Physiscs Department, Indian Institute of Technology Delhi, 110016, India. E-mail: mageshkumar2006@gmail.com

acceleration. They found that in tapered plasma channel the dephasing length is increased relative to the untapered channels, and larger energy gains are achieved. Rowlands-Rees *et al.* (2008) generated quasimonoenergetic electron beams with energies up to 200 meV in a partially ionized plasma channel by laser plasma accelerator driven in a hydrogen-filled capillary discharge waveguide. Singh (2009) have studied the effect of the radial and temporal profile of laser pulse on acceleration of electrons generated during the ionization of krypton and have shown that the beam quality can be improved by using a nearly flat radial profile.

In this paper, we develop a model of laser wakefield electron acceleration in the blow out regime in a pre-existing non-uniform plasma channel. The picture of blow out regime electron acceleration is as follows. An intense short pulse, with pulse duration of the plasma period ω_p^{-1}, spot size w_0 on the order of c/ω_p, (where c is the speed of light in free space), and normalized amplitude a_0, exerts axial, and radial ponderomotive force on the plasma electrons creating an ion bubble co-moving with the laser pulse. The bubble radius has a correlation with the laser spot size and laser amplitude. In the moving bubble frame, the expelled electrons on reaching the bubble boundary move backward and return to the stagnation point at the rear of the bubble on laser axis. The accumulated electron charge at the stagnation point slows down the surging electrons, brings them to rest in the bubble frame. These electrons are then pulled into the ion bubble by the ion space charge field. We calculate the energy gain of a test electron in aforementioned bubble regime with radial density profile in a Lorentz boosted frame (Vay, 2007) (bubble frame in which the quasi-static sphere acquires an elliptic shape (Thomas, 2010)).

In section 2, we consider the dynamics of an electron initially near the channel axis, hit by a laser pulse with Gaussian intensity distribution. We obtain the trajectories of the laser expelled electrons by solving the equations of motion and compared the results with PIC simulations. We estimate the radial extent of the bubble equating ponderomotive and space charge force at the bubble boundary. Also the radius of the electron sphere is assessed by equating potential energy of the electrons at the pile surface at the stagnation point to their initial kinetic energy. In Section 3, we estimate the energy gain of an electron as it moves from the stagnation point to the center of the ion bubble. In section 4, we summarize our conclusions and in Appendix A, we have shown the calculation of the longitudinal space charge field E_z' in the moving frame.

2. ION BUBBLE IN A PREFORMED PLASMA CHANNEL: A DYNAMIC APPROACH

Consider a preformed plasma channel with ion (or electron) density profile,

$$n_0 = n_0^0(1 + r^2/r_{ch}^2), \tag{1}$$

where r_{ch} is the radius of the channel and n_0^0 is the density at the channel axis. An intense short pulse laser propagates through it,

$$\begin{aligned} \mathbf{E}_L &= \mathbf{A}_L(r, z, t)e^{-i(\omega t - kz)}, \\ A_L^2 &= A_{00}^2 e^{-r^2/w_0^2} e^{-\zeta^2/v_g^2\tau^2}, \end{aligned} \tag{2}$$

where $k = \omega/c(1-\omega_p^2/\omega^2)^{1/2}$, $v_g = c(1-\omega_p^2/\omega^2)^{1/2}$, $\zeta = z - v_g\, t$, $\omega_p = k_p c = \sqrt{4\pi n_0^0 e^2/m}$, $-e$ and m are the electron charge and mass. It exerts a ponderomotive force on electrons,

$$\mathbf{F} = e\nabla\phi_p = \frac{ma^2c^2}{2\gamma}\left[\frac{r}{w_0^2}\hat{r} + \frac{\zeta}{v_g^2\tau^2}\hat{z}\right], \tag{3}$$

where $\phi_p = -(mc^2/e)(\gamma - 1)$, $\gamma = \sqrt{1 + \frac{1}{2}a^2}$, $a^2 = a_0^2 e^{-r^2/w_0^2} e^{-\zeta^2/v_g^2\tau^2}$, and $a_0 = eA_{00}/m\omega c$.

As the electron originated at r_i (initial point) at time $t = 0$ moves to a distance r, it sees the space charge field due to the ion space charge left behind. The net ion charge in a cylinder of radius r and unit axial length is $2\pi\int_0^r n_0^0 e(1 + r^2/r_{ch}^2)rdr$. Therefore, the space charge field may be approximated as,

$$E_r = \frac{n_0^0 e(r^2 - r_i^2)}{2\epsilon_0 r} + \frac{n_0^0 e(r^4 - r_i^4)}{4\epsilon_0 r_{ch}^2 r}, \tag{4}$$

while the longitudinal component of space charge field, which is Lorentz invariant, is $E_z = E_z'$ (where E_z' is the field in moving frame, as calculated in Appendix A). In addition, to these transverse fields an azimuthal magnetic field $B_\phi = -E_r/c$ is also generated within the cavity moving with relativistic velocities (Lu *et al.*, 2006; Kostyukov *et al.*, 2010; Lotov, 2004). In the quasi-equilibrium, as the laser bubble combine moves ahead, the plasma electrons must remain outside the bubble, at the bubble boundary or bit farther from it. Simulations reveal that the width of the region of electron build up at the boundary is significantly smaller than the radius of the bubble. Since the axial velocities of electrons in this layer are less than v_g (the velocity of the bubble), these electrons surge toward the stagnation point near the bubble. We may get a reasonable clue about the shape of the bubble by studying the trajectory of a test electron that originates at an off axis point at the front of the laser pulse. The equation of motion for the electron in the laboratory frame in component form can be written as,

$$\frac{d(\gamma v_r)}{dt} = \frac{F_r}{m} - \frac{e(E_r - v_z B_\phi)}{m}, \tag{5}$$

$$\frac{d(\gamma v_z)}{dt} = \frac{F_z}{m} - \frac{e(E_z + v_r B_\phi)}{m}. \tag{6}$$

Writing $d(\gamma\vec{v})/dt = \vec{v}d\gamma/dt + \gamma d\vec{v}/dt$, where $\vec{v} = v_r\hat{r} + v_z\hat{z}$

https://doi.org/10.1017/S0263034612000547 Published online by Cambridge University Press

and $d\gamma/dt = -\frac{a^2}{2\gamma}\left[\frac{r}{w_0^2}\frac{dr}{dt} + \frac{\zeta}{v_g^2\tau^2}(v_z - v_g)\right]$, one obtains,

$$\frac{d^2r}{dt^2} = \frac{F_r}{m\gamma} - \frac{e(E_r - v_z B_\phi)}{m\gamma} + \frac{a^2}{2\gamma^2}\frac{dr}{dt}\left[\frac{r}{w_0^2}\frac{dr}{dt} + \frac{\zeta}{v_g^2\tau^2}(v_z - v_g)\right], \quad (7)$$

$$\frac{d^2z}{dt^2} = \frac{F_z}{m\gamma} - \frac{e(E_z + v_r B_\phi)}{m\gamma} + \frac{a^2}{2\gamma^2}\frac{dz}{dt}\left[\frac{r}{w_0^2}\frac{dr}{dt} + \frac{\zeta}{v_g^2\tau^2}(v_z - v_g)\right], \quad (8)$$

where F_r and F_z are the radial components of ponderomotive force obtained from Eq. (3).

To estimate the efficacy of the dynamic approach, we numerically solved the coupled Eqs. (7) and (8) for the parameters used by Mora (2009), $a_0 = 5$, the spot size $k_p\, w_0 = 2.5$ and the pulse length $k_p v_g \tau = 6$, where $v_g = c\sqrt{1 - (1/\gamma_g^2)} \approx 0.995c$ for $\gamma_g = 10$. Mora used fully relativistic time-averaged particle code WAKE to study the radial wavebreaking of the density perturbation in the highly nonlinear laser wakefield regime in a uniform plasma. Figure 1a shows the contours of electron trajectories of analytically obtained by us for electrons starting from different radial positions $k_p\ r_i = 0.3$, 0.6, 0.8, and 1. One may note that the electrons (in the moving bubble) are streaming backward from right to left. All the trajectories tend to converge at the rear (at $k_p(z - v_g\, t) = -11$) and acquire a spherical shape. This is indicative of longitudinal wavebreaking. For comparison, we have in Figure 1b the trajectories obtained by Mora (2009) in their simulations. Their trajectories run from left to right due to horizontal axis being $k_p(ct - z)$. For the electron originating near the axis, the trajectories diverge continuously away from the axis. For the electrons originating between $k_p r_i \sim 1.3$ and 3, the trajectories surge to a common radial point and then bend toward the z axis. The ones between $k_p r_i = 1.3$ and 1.8 reach the axis at $k_p(ct - z) \approx 10$, which is comparable to axial span of trajectories inour case (Fig. 1a). The radial height of these trajectories (the radial breaking point) is $k_p r_i \sim 3$ that is close to the height of trajectories in our case. The major difference is in the trajectories of electrons for $k_p r_i < 1$.

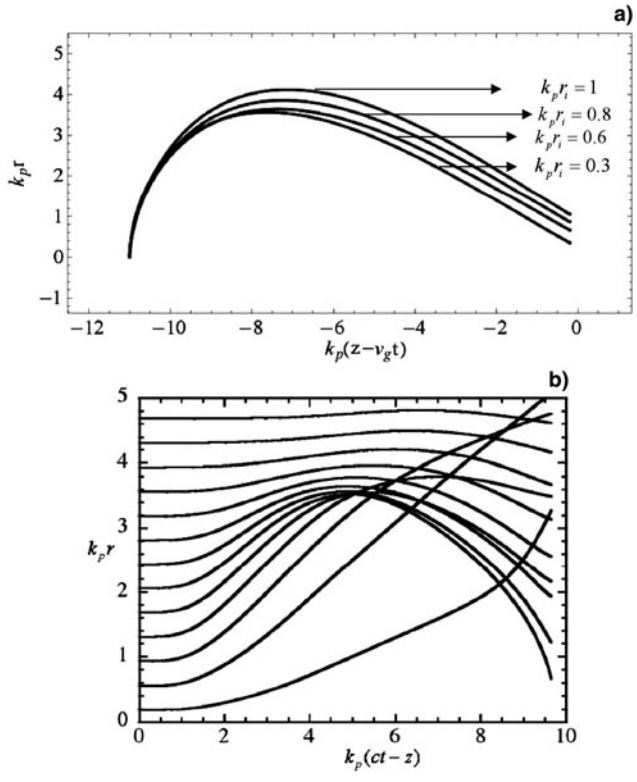

Fig. 1. Contour of $k_p r$ with $k_p(z - v_g t)$ for $a_0 = 5$, $k_p w_0 = 2.5$, $k_p v_g \tau = 6$ and $k_p r_i = 0.3$, 0.6, 0.8 and where $v_g = 0.995c$. Figure 1b is printed with permission from Patrick Mora (*Eur. Phys. J. Special Topics* 175, 97–104 (2009).

Similarly, Kim *et al.* (2003) used a two-dimensional PIC simulation to study the electron trapping and acceleration of electrons in the bubble (wakefield) with parabolic density profile. The parameters used were: $a_0 = 2.27$, the laser wavelength $\lambda = 0.8\ \mu m$, the minimum density at the axis $n_0^0 = 2.1 \times 10^{18}\ \mathrm{cm}^{-3}$, corresponding plasma wavelength $\lambda_p = 23.21\ \mu m$, the pulse duration $\tau = 50$ fs and the pulse length $k_p v_g \tau = 4$, where $v_g \approx 0.998c$ for $\gamma_g = \lambda_p/\lambda \approx 30$. The spot size at the centre of the channel is $w_0 = 10\ \mu m$ ($k_p w_0 = 2.7$) and the channel radius is $r_{ch} = 160\ \mu m$ ($k_p r_{ch} = 43.3$). The wake has taken the form of a bubble with longitudinal dimension $\Delta z = 25\ \mu m$, where as the radius is $\approx 8\ \mu m$ at $z = 100\ \mu m$ and the accelerated electron bunch gains energy in the ranges of 5 and 20 MeV.

Now we compare our result by solving the same coupled equations Eqs. (7) and (8) in the lab frame for the parameters mentioned above. Figure 2 shows the contour of electron trajectory for $k_p r_i = 0.1$. One may note that the radiusof the bubble is approximately equal to 9 μm and the longitudinal extent is $\approx 30\ \mu m$ that are not too different from the value of 8 μm and 25 μm obtained in PIC simulations. A detailed analysis of energy gain of a test electron will be discussed later.

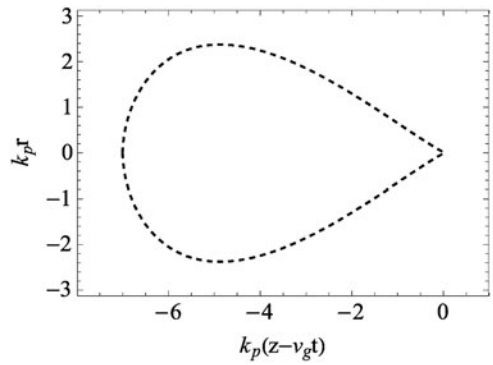

Fig. 2. Contour of $k_p r$ with $k_p(z - v_g t)$ for $a_0 = 2.27$, $k_p w_0 = 2.7$, $k_p r_{ch} = 43.2$, $k_p v_g \tau = 4$ and $k_p r_i = 0.1$, where $v_g = 0.998c$.

https://doi.org/10.1017/S0263034612000547 Published online by Cambridge University Press

The trajectory of the laser expelled electrons is entirely different in a frame moving parallel to the bubble. One may use the Lorentz transformation, $z' = \gamma_g(z - v_g t)$ and $t = \gamma_g(t' + v_g z'/c^2)$ (primed variables representing the moving frame) to transform the equations Eqs. (7) and (8) from lab frame to Lorentz boosted frame. Therefore,

$$\frac{d^2z'}{dt'^2} = \frac{a^2}{2\gamma^2}\gamma_g^2\left[\frac{z'}{L_p^2}\left(1+\frac{v_g v_z'}{c^2}\right)^3 + \left(\frac{v_g}{c}\right)^2\left(1+\frac{v_z'}{v_g}\right) \times\left(\frac{r}{R_0^2}\frac{v_r'}{v_g} + \frac{z'}{\gamma_g^2 L_p^2}\frac{v_z'}{v_g}\right)\right] - \gamma_g^3\left(1+\frac{v_g v_z'}{c^2}\right)^3 \times\left(\frac{eE_z'}{m\gamma\omega_p c} - \frac{v_r'}{c}\left(\frac{(r^2-r_{in}^2)}{2\gamma r} + \frac{(r^4-r_{in}^4)}{4\gamma R_{ch}^2 r}\right)\right), \tag{9}$$

$$\frac{d^2r}{dt'^2} = \frac{a^2}{2\gamma^2}\left(\frac{r}{R_0^2}\left(\left(1+\frac{v_g v_z'}{c^2}\right)^2 + \frac{v_r'^2}{c^2}\right) + \frac{z'}{\gamma_g^2 L_p^2}\frac{v_r' v_z'}{c^2} + \frac{v_r' v_g}{c^2}\frac{v_z'}{(1+\frac{v_g v_z'}{c^2})} - \gamma_g^2\left(1+\frac{v_g v_z'}{c^2}\right)^2\left(\frac{(r^2-r_{in}^2)}{2\gamma r} + \frac{(r^4-r_{in}^4)}{4\gamma R_{ch}^2 r}\right)\left(1+\frac{v_z'}{c}\right)\right), \tag{10}$$

where $r \to k_p r$, $r_{in} \to k_p r_i$, $R_0 \to k_p w_0$, $R_{ch} \to k_p r_{ch}$, $z' \to k_p z'$, $t' \to \omega_p t'$, $v_r' = dr/dt'$, $v_z' = dz'/dt'$, $L_p = k_p v_g \tau$, $\gamma_g = (1 - v_g^2/c^2)^{-1/2}$, and $v_g \to v_g/c$ (v_g is the velocity of the frame moving parallel to the ion bubble). The coupled Eqs. (9) and (10) are numerically solved to obtain the trajectory of the electrons in the Lorentz boosted frame. Figure 3 represents the contour of the electron trajectory in the moving frame plotted for the parameters used by Kim *et al.* (2003) From Figure 3 one may note that the longitudinal distance is approximately stretched to γ_g ($\approx$30) times the transverse dimension of the bubble with maximum radius at the centre. Hence the ion bubble acquires an elliptic shape in the Lorentz boosted frame moving parallel to the bubble.

Previous studies (Esarey *et al.*, 2009; Lu *et al.*, 2006; Kostyukov *et al.*, 2010) have given an estimate of the radius of ion bubble by equating the laser ponderomotive force on a single electron and ion channel force for a uniform plasma. Following the same analysis, one may estimate the maximum radius of the non uniform ion bubble by balancing the two forces at the bubble boundary in the lab frame.

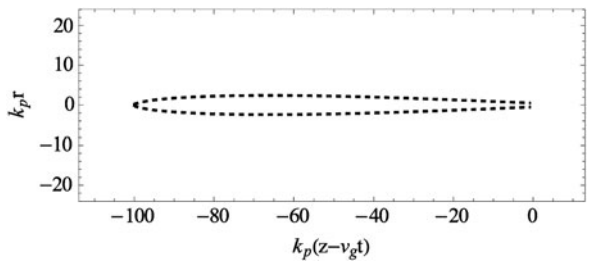

Fig. 3. Contour of $k_p r$ with $k_p(z - v_g t)$ in the Lorentz boosted frame for $a_0 = 2.27$, $k_p w_0 = 2.7$, $k_p r_{ch} = 43.2$, $k_p v_g \tau = 4$ and $k_p r_i = 0.1$, where $v_g = 0.998c$.

From the Poisson's equation $\nabla^2\phi = e(n_e - n_0)/\epsilon_0$, on using $\phi = -\phi_p$ and $n_e = 0$ (complete evacuation of electrons inside the ion bubble) one obtains the bubble boundary $r \equiv R$ versus $Z_1 = \zeta$, $\zeta = z - v_g t$,

$$1 + \frac{R^2}{r_{ch}^2} - \frac{a^2/2}{(1+a^2/2)^{3/2}}\left[\left(\frac{2(1-R^2/w_0^2)+(a^2/2)}{k_p^2 w_0^2}\right)(2-R^2/w_0^2) - \left(\frac{(1-2Z_1^2/(v_g^2\tau^2)+(a^2/2)}{k_p^2(v_g^2\tau^2)}\right)(1-Z_1^2/(v_g^2\tau^2))\right] = 0, \tag{11}$$

where $a^2 = a_0^2 e^{-R^2/w_0^2} e^{-Z_1^2/(v_g\tau)^2}$, R is the radius, and ϕ is the space charge potential of the ion bubble.

Inside the bubble $\phi \neq -\phi_p$ and imbalance of the ponderomotive and space charge forces does not matter as there are no electrons to feel the forces. The bubble surface in the moving frame is an ellipsoid with axial length $L_z = \gamma_g\zeta(=z - v_g t)$ (at $R = 0$) and transverse length $L_r = R$ (at $Z_1 = 0$). Substituting $Z_1 = 0$ and $r = L_r$ in Eq. (11) we obtain,

$$\left(1+\frac{L_r^2}{r_{ch}^2}\right)(2+a'^2)^{1/2} = \sqrt{2}\frac{a'^2}{k_p^2 w_0^2}\left[1 + \frac{w_0^2}{2v_g^2\tau^2} - \frac{L_r^2}{2w_0^2}\frac{4+a'^2}{2+a'^2}\right], \tag{12}$$

where $a'^2 = a_0^2 e^{-L_r^2/w_0^2}$.

The transverse dimension L_r (maximum radius) of the ion bubble is a function of laser amplitude a_0, spot size w_0, channel dimension r_{ch}, and pulse width τ. For a long laser pulse $w_0/v_g\tau \ll 1$, i.e., pulse length larger than the spot size, L_r is independent of τ. However, for a short pulse L_r has dependence on τ. Eq. (12) is transcendental equation and is numerically solved for L_r. Figure 4 shows the variation of transverse

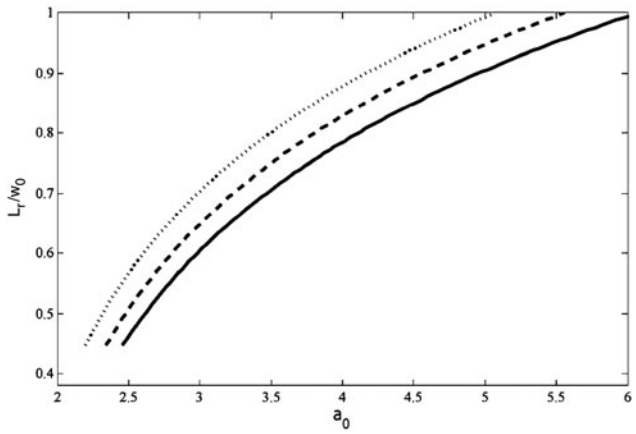

Fig. 4. Variation of L_r/w_0 with a_0 for $w_0/r_{ch} = 0.7$ (dot), 0.8 (dash) and 0.9 (solid), where $k_p r_{ch} = 3$ and $w_0/v_g\tau = 0.32$.

https://doi.org/10.1017/S0263034612000547 Published online by Cambridge University Press

length L_r/w_0 with a_0 for $k_p r_{ch} = 3$ and $w_0/v_g\tau = 0.32$. The transverse size of the bubble initially rises almost linearly with a_0 and then tends to saturate at a value comparable to laser spot size. For $a_0 = 3$, $k_p w_0 = 2.1$, and $k_p r_{ch} = 3$ the radius L_r turns out to be $L_r = 1.5c/\omega_p$. For a constant value of L_r, i.e., to achieve a bubble of a given radius, the laser spot size $k_p w_0$ varies linearly with a_0.

It is also possible to estimate the critical size $k_p r_e$ of the electron sphere at the stagnation point by equating the potential energy (potential $= n_e e r_e^2/3\epsilon_0$) of the electrons at the surface of the electron sphere to their initial kinetic energy at the bubble boundary (after emerging from the laser) (Liu & Tripathi, 2010). So one obtains,

$$\begin{aligned} n_e r_e^2 e^2/3\epsilon_0 &= mc^2(\gamma_{in} - 1) \\ \Rightarrow k_p r_e &\sim \sqrt{3(\gamma_{in} - 1)/n}, \end{aligned} \tag{13}$$

where $\gamma_{in}^2 = (1 - v_{in}^2/c^2)^{-1}$, v_{in}/c is the initial velocity of the electron just after emerging from the laser and $n = n_e/n_0^0$. The critical size of electron sphere thus depends upon the initial energy and ratio of densities n. For $v_{in}/c = 0.99$, $n = 100$, one obtains $k_p r_e = 0.5$.

3. ENERGY GAIN

Now we calculate the energy gained by a test electron under the influence of the longitudinal field $E_z^{'}$ of the ion bubble in the Lorentz boosted frame. The longitudinal electric field E_z' (see Appendix A) depends on radius $R(a_0, v_g\tau, w_0, r_{ch})$ and z_m. Figure 5 shows the variation of E_z' with $z_m/\gamma_g R$ for different values of a_0, where z_m is the distance (from the shifted origin) on the longitudinal axis of the ion bubble. The longitudinalfield is almost linear and symmetric about the center of the cavity. For $a_0 = 3.27$, $k_p w_0 = 6.28$, $k_p v_g\tau = 4.2$, where $v_g = 0.996c$ and $\gamma_g = 16.3$, the acceleration gradient is $E_z' \sim 6$ GV/cm for uniform density 6.5×10^{18} cm^{-3} (parameters from Kalmykov *et al.* (2011). Therefore, the bubble provides a huge space charge potential, which pulls the electrons from the stagnation point with a huge force eE_z'. Hence a test electron in the spherical electron cloud at the stagnation point can gain tremendous amount of energy.

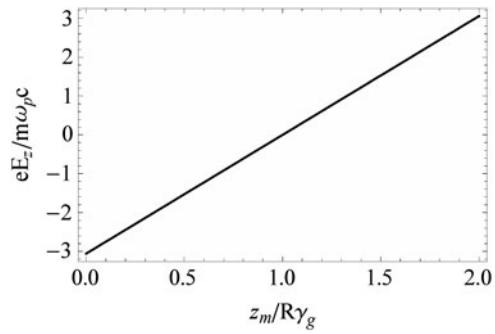

Fig. 5. Variation of longitudinal field $eE_z'/m\omega_p c$ inside the uniform bubble with $z_m/\gamma_g R$ for $a_0 = 3.27$, $k_p w_0 = 6.28$ and $k_p v_g\tau = 4.2$, where $v_g = 0.996c$.

Using energy gain equation, one may write

$$\frac{d\gamma'}{dt'} = -\frac{eE_z' v_z}{m_0 c^2}, \tag{14}$$

where γ', $v_z = dz_m/dt'$ (longitudinal velocity of electron inside the ion bubble) and t' are measured in boosted frame. Transforming from moving frame to lab frame, using Lorentz transformations, we get

$$\gamma_{lab} = \gamma_g\left(\gamma' + (v_g/c)\sqrt{\gamma'^2 - 1}\right), \tag{15}$$

$$dt/dt' = \gamma_g. \tag{16}$$

Eq. (14) is numerically solved using fourth order Runga Kutta method and transformed to lab frame using Eqs. (15) and (16). Variation of electron energy (MeV) with $z_m/\gamma_g R$ is plotted in Figure 6 for the parameters used by (2003) (red) and Chen *et al.* (2010) (blue). Chen *et al.* (2010) performed 2D PIC simulation to obtain the dependence of the maximum energy of the electron beam on laser amplitude a_0 and plasma density. Their simulation shows that the maximum energy of the electron beam varies from 90–200 MeV in the density range $3\text{–}4\times10^{19}$ cm^{-3} for the initial laser amplitude $a_0 = 4$, initial spot size $w_0 = 4$ μm, pulse length $c\tau =$ 13.5 μm and laser wavelength $\lambda = 0.8$ μm. For a comparison we have in Figure 6 the energy gain of the test electron in the density regime of Chen's *et al.* (2010) simulation. Figure 6 shows the variation of energy gain of a test electron with $z_m/\gamma_g R$ for uniform and nonuniform plasma density. One may note that the test electron gains a maximum energy of about 35 (dash) and ≈100 (Solid) MeV before entering the dephasing region of the ion bubble. Since the longitudinal field of the bubbleis approximately linear about the center of the bubble (shown in Fig. 5), the electron that crosses the center of the ion bubble are decelerated due to the reversal of sign of the longitudinal field. Hence the interaction must terminate there. The energygains obtained for the both cases are in reasonable agreement with the previous studies.

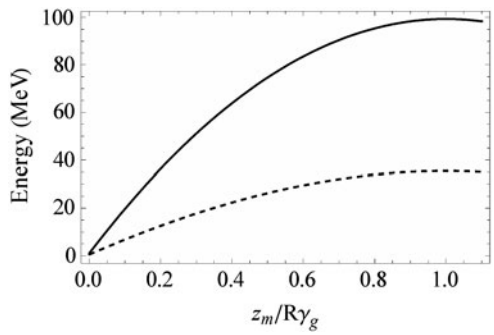

Fig. 6. Variation of electron energy with $z_m/\gamma_g R$ for uniform and non uniform plasma. The parameters for non uniform plasma (dash): $a_0 = 2.27$, $k_p w_0 = 2.7$, $k_p r_{ch} = 43.2$, $k_p v_g\tau = 4$, $v_g = 0.998c$ and laser wavelength $\lambda = 0.8$ μm. And for uniform plasma (solid): $a_0 = 4$, $k_p w_0 = 4.48$, $k_p v_g\tau = 15.45$, $v_g = 0.99c$ and laser wavelength $\lambda = 0.8$ μm.

https://doi.org/10.1017/S0263034612000547 Published online by Cambridge University Press

Though the model which we use did not include the effects of laser pulse evolution nor self-focusing and electron beam loading on the plasma bubble, it gives an estimate of energy gain of electrons within a factor of 1.5 or 2 from simulation results.

4. CONCLUSIONS

The bubble regime wakefield acceleration depends on the bubble radius R and bubble charge density n_0^0. The transverse size of the bubble rises almost linearly with a_0 in the range of $a_0 = 1$–3.5, and then tends to saturate at a value comparable to laser spot size. The contour of the laser expelled electrons and the energy gain obtained analytically are found to be in reasonable agreement with PIC simulations. The radius of the electron pile at the stagnation point obtained by equating the potential energy of the electrons at the pile surface to their kinetic energy at the bubble boundary is small. Electric field profile of ion bubble is found to be linear and symmetric about the center of the cavity. Therefore electrons will be accelerated in the first half phase before entering the decelerating phase. The Lorentz boosted frame enabled us to calculate energy gain of a test electron inside the bubble.

ACKNOWLEDGEMENT

One of the authors, Magesh would like to thank IIT Delhi for financial support.

REFERENCES

Amirano, F., Baton, S., Bernard, D., Cros, B., Descamps, D., Dorchies, F., Jacquet, F., Malka, V., Marqus, J.R., Matthieussent, G., Min, P., Modena, A., Mora, P., Morillo, J. & Najmudin, Z. (1998). Observation of laser wakefield acceleration of electrons. *Phys. Rev. Lett*. **81**, 995–998.

Balakirev, V.A., Karas, I.V., Karas, V.I., Levchenko, V.D. & Bornatici, M. (2004). Charged particle acceleration by an intense wake-field excited in plasmas by either laser pulse or relativistic electron bunch. *Laser Part. Beams* **22**, 383–392.

Chen, S.H., Tai, L.C., Liu, C.S. & Lin-Liu, Y.R. (2010). Beam energy scaling of a stably operated laser wakefield accelerator. *Phys. Plasmas* **17**, 063109–06311.

Chen, Z.L., Unick, C., Vafaei-Najafabadi, N., Tsui, Y.Y., Fedosejevs, R., Naseri, N., Masson-Laborde, P.-E. & Rozmus, W. (2008). Quasi-monoenergetic electron beams generated from 7 TW laser pulses in N_2 and He gas targets. *Laser Part. Beams* **26**, 147–155.

Dahiya, D., Sajal, V. & Sharma, A.K. (2010). Self-injection of electrons in a laser-wakefield accelerator by using longitudinal density ripple. *Appl. Phys. Lett.* **96**, 021501–021503.

Esarey, E., Schroeder, C.B. & Leemans, W.P. (2009). Physics of laser-driven plasma-based electron accelerators. *Rev. Mod. Phys*. **81**, 1229–1285.

Faure, J., Glinec, Y., Pukhov, A., Kiselev, S., Gordienko, S., Lefebvre, E., Rousseau, J.P., Burgy, F. & Malka, V. (2004). A laser-plasma accelerator producing monoenergetic electron beams. *Nat*. **431**, 541–544.

Geddes, C.G.R., Toth, C.S., Tilborg, J.V., Esarey, E., Schroeder, C.B., Bruhwiler, D., Nieter, C., Cary, J. & Leemans, W.P. (2004). Monoenergetic beams of relativistic electrons from intense laser-plasma interactions. *Nat*. **431**, 535–538.

Glinec, Y., Faure, J., Pukhov, A., Kiselev, S., Gordienko, S., Mercier, B. & Malka, V. (2005). Generation of quasi-monoenergetic electron beams using ultrashort and ultraintense laser pulses. *Laser and Particle Beams* **23**, 161–166.

Gorbunov, L.M., Kalmykov, S.Yu. & Mora, P. (2005). Laser wakefield acceleration by petawatt ultrashort laser pulses. *Phys. Plasmas* **12**, 033101–033110.

Hogan, M.J., Barnes, C.D., Clayton, C.E., Decker, F.J., Deng, S., Emma, P., Huang, C., Iverson, R.H., Johnson, D.K., Joshi, C., Katsouleas, T., Krejcik, P., Lu, W., Marsh, K.A., Mori, W.B., Muggli, P. O'connell, C.L., Oz, E., Siemann, R.H. & Walz, D. (2005). Multi-GeV energy gain in a plasma-wakefield accelerator. *Phys. Rev. Lett.* **95**, 054802–054805.

Kalmykov, S.Y., Beck, A., Yi, S.A., Khudik, V.N., Downer, M.C., Lefebvre, E., Shadwick, B.A. & Umstadter, D.P. (2011). Electron self-injection into an evolving plasma bubble: Quasi-monoenergetic laser-plasma acceleration in the blowout regime. *Phys. Plasmas* **18**, 056704–056712.

Kim, J.U., Kim, C., Kim, G.H., Hafz, N., Lee, H.J. & Suk, H. (2003). A simulation for electron trapping and acceleration in parabolic density profile and ongoing experimental plan. *Proceedings of the 2003 Particle Accelerator Conference* 3, 1849–1851.

Kostyukov, I., Pukhov, A. & Kiselev, S. (2010). Phenomenological theory of laser-plasma interaction in "bubble" regime. *Phys. Plasmas* **11**, 5256–5264.

Krishnagopal, S., Samant, S.A., Sarkar, D., Upadhyay, A.K. & Jha, P. (2011). *Study of Self-injection of an Electron Beam in a Laser-driven Plasma Cavity*, Proceedings of IPAC2011. San Sebastin, Spain.

Liu, C.S. & Tripathi, V.K. (2010). Charged particle acceleration by lasers in plasmas. *AIP Conf. Proc*. 920, 76–97.

Lotov, K.V. (2004). Blowout regimes of plasma wakefield acceleration. *Phys. Rev. E* **69**, 046405–046417.

Lu, W., Huang, C., Zhou, M., Tzoufras, M., Tsung, F.S., Mori, W.B. & Katsouleas, T. (2006). A nonlinear theory for multidimensional relativistic plasma wave wakefields. *Phys. Plasmas* **13**, 056709–056721.

Lu, W., Tzoufras, M., Joshi, C., Tsung, F.S., Mori, W.B., Vieira, J., Fonseca, R.A. & Silva, L.O. (2007). Generating multi-GeV electron bunches using single stage laser wakefield acceleration in a 3D nonlinear regime. *Phys. Rev. ST Accel.Beams* **10**, 061301–061312.

Maksimchuk, A., Reed, S., Bulanov, S.S., Chvykov, V., Kalintchenko, G., Matsuoka, T., Mcguffey, C., Mourou, G., Naumova, N., Nees, J., Rousseau, P., Yanovsky, V., Krushelnick, K., Matlis, N.H., Kalmykov, S., Shvets, G., Downer, M.C., Vane, C.R., Beene, J.R., Stracener, D. & Schultz, D.R. (2008). Studies of laser wakefield structures and electron acceleration in underdense plasmas. *Phys. Rev. Lett*. **15**, 056703–056710.

Martins, S.F., Fonseca, R.A., Lu, W., Mori, W.B. & Silva, L.O. (2010). Exploring laser-wakefield-accelerator regimes for near-

term lasers using particle-in-cell simulation in Lorentz-boosted frames. *Nat. Phys*. **6**, 311–316.

Mora, P. (2009). Particle acceleration in ultra-intense laser plasma interaction. *Eur. Phys. J. Special Topics* **175**, 97–104.

Pukhov, A. & Meyer-Ter-Vehn, J. (2002). Laser wake field acceleration: the highly non-linear broken-wave regime. *Appl. Phys. B: Lasers Opt*. **74**, 355–361.

Reitsma, A.J.W. & Jaroszynski, D.A. (2004). Coupling of longitudinal and transverse motion of accelerated electrons in laser wakefield acceleration. *Laser Part. Beams* **22**, 407–413.

Rowlands-Rees, T.P., Kamperidis, C., Kneip, S., Gonsalves, A.J., Mangles, S.P.D., Gallacher, J.G., Brunetti, E., Ibbotson, T., Murphy, C.D., Foster, P.S., Streeter, M.J.V., Budde, F., Norreys, P.A., Jaroszynski, D.A., Krushelnick, K., Najmudin, Z. & Hooker, S.M. (2008). Laser-driven acceleration of electrons in a partially ionized plasma channel. *Phys. Rev. Lett.* **100**, 105005–105008.

Sadighi-Bonabi, R., Navid, H.A. & Zobdeh, P. (2009). Observation of quasi mono-energetic electron bunches in the new ellipsoid cavity model. *Laser Part. Beams* **27**, 223–231.

Siders, C.W., Le Blanc, S.P., Fisher, D., Tajima, T., Downer, M.C., Babine, A., Stepanov, A. & Sergeev, A. (1996). Laser wakefield excitation and measurement by femtosecond longitudinal interferometry. *Phys. Rev. Lett.* **76**, 3570–3573.

Singh, A. & Singh, N. (2011). Relativistic guidance of an intense laser beam through an axially non-uniform plasma channel. *Laser Part. Beams* **29**, 291–298.

Singh, K.P. (2009). Acceleration of electrons generated during ionization of a gas by a nearly flat profile laser pulse. *Phys. Plasma* **16**, 093103–093108.

Sprangle, P., Hafizi, B., Peano, J.R., Hubbard, R.F., Ting, A., Moore, C.I., Gordon, D.F., Zigler, A., Kaganovich, D. & Antonsen Jr., T.M. (2001). Wakefield generation and GeV acceleration in tapered plasma channels. *Phys. Rev. E* **f63**, 056405–056415.

Tajima, T. & Dawson, J.M. (1979). Laser electron accelerator. *Phys. Rev. Lett*. **43**, 267–270.

Thomas, A.G.R. (2010). Scalings for radiation from plasma bubbles. *Phys. Plasmas* **17**, 056708–056719.

Vay, J.L. (2007). Noninvariance of space- and time-scale ranges under a Lorentz transformation and the implications for the study of relativistic interactions. *Phys. Rev. Lett*. **98**, 130405–130408.

Verma, U. & Sharma, A.K. (2011*a*). Nonlinear electromagnetic Eigen modes of a self created magnetized plasma channel and its stimulated Raman scattering. *Laser Part. Beams* **29**, 471–477.

Verma, U. & Sharma, A.K. (2011*b*). Laser focusing and multiple ionization of Ar in a hydrogen plasma channel created by a prepulse. *Laser Part. Beams* **29**, 219–225.

APPENDIX

A. AXIAL SPACE CHARGE FIELD OF AN ELLIPSOIDAL ION BUBBLE

In this appendix, we will derive the expression for the longitudinal space charge field (E_z') in the moving frame following the analysis (Thomas, 2010), supported by PIC simulation (Martins *et al.*, 2010). Therefore, we choose the ion bubble as an ellipsoid with transverse dimension $L_r = 2R$ and longitudinal $L_z \cong 2R\gamma_g$ in a frame moving with velocity v_g parallel to the bubble. The ion bubble has a radial density profile with minimum on the axis. Shifting the origin of the ion bubble by a distance $-L_z/2$ to the bubble rear (see Fig. 7), the longitudinal field E_z' inside the cavity is obtained by dividing the ellipsoid into many plates of thickness dl and radius $r_l = (L_r/L_z)\sqrt{(L_z/2)^2 - (L_z/2 - l)^2}$. Therefore, the electric field inside the bubble at a distance z_m (from the shifted origin) on the longitudinal axis of ellipsoid is,

$$E_z' = \frac{m\omega_p^2}{2e\gamma_g}\int_0^{L_z}\int_0^{r_l}\frac{(1 + r^2/r_{ch}^2)(z_m - l)rdrdl}{(r^2 + (z_m - l)^2)^{3/2}}. \tag{17}$$

Avoiding the intermediate steps one may finally write,

$$\frac{eE_z'}{m\omega_p c} = -R(1 - y) - \frac{R^3\gamma_g^2}{6r_{ch}^2}(3 + y)((2 - y)^3 - y^3), \tag{18}$$

where $y = z_m/R\gamma_g$ and $R \rightarrow R\omega_p/c$. The radius of the ion bubble R is obtained by solving Eq. (12) for the parameters a_0, w_0, r_{ch} and $v_g\tau$.

Similarly one may obtain the radial field E_r , but its value is zero at the axis by symmetry. The radial field focusses the electron bunch accelerated by the space charge thus reducing the transverse spread. So the axial and off axis electrons gain energy only because of the longitudinal force (eE_z').

B. MAGNETIC VECTOR POTENTIAL OF THE ION BUBBLE

In the laser group velocity frame the ion bubble has current density,

$$J_z = -nev_g. \tag{19}$$

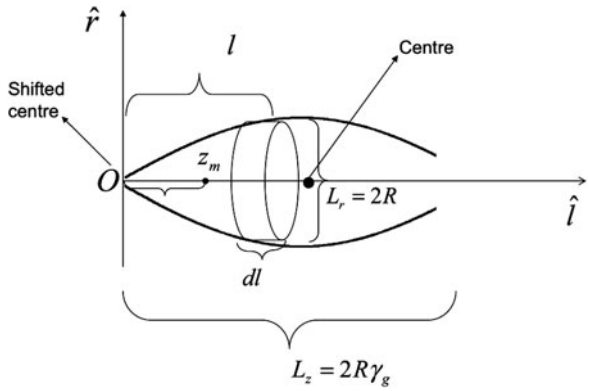

Fig. 7. Schematic of Ellipsoid.

https://doi.org/10.1017/S0263034612000547 Published online by Cambridge University Press

Let in the moving frame the center of the spherical bubble be at the origin. On the axial point (0,0,z) one writes,

$$A_z(z) = \frac{\mu_0}{4\pi} \int_{-R}^{R} \int_{z'}^{\sqrt{R^2-z'^2}} \frac{J_z}{R'} 2\pi r' dr' dz', \tag{20}$$

where R is the radius of the sphere, $R' = |z\hat{z} - \sqrt{r'^2 - z'^2}\hat{x} - z'\hat{z}| = ((z-z')^2 + r'^2 - z'^2)^{1/2}$ and r' and z' represents the position coordinates of the source point measured from the center. Substituting the values of J_z and R', the above equation becomes,

$$A_z(z) = -\frac{\mu_0 n e v_g}{2} \int_{-R}^{R} \int_{z'}^{\sqrt{R^2-z'^2}} \frac{2\pi r' dr' dz'}{(z^2 + r'^2 - 2zz')^{1/2}}. \tag{21}$$

Thus on the axis ($r = 0$) the magnetic field $B = \nabla \times \vec{A}$ is zero. The same would hold for an ellipsoidal bubble.

https://doi.org/10.1017/S0263034612000547 Published online by Cambridge University Press